

PAPER • OPEN ACCESS

Measurement-induced heating of a trapped ion

To cite this article: A J Rasmusson et al 2024 J. Phys. B: At. Mol. Opt. Phys. 57 225002

View the article online for updates and enhancements.

You may also like

- Smallholder RSPO certification, economic benefits and agrochemical use Sebastian Renner, Anette Ruml, Tabea Lakemann et al.
- Computational investigation of transport parameters of ions in gas-filled radiation detectors

Yalçn Kalkan, Sedat Ar, Salim Orak et al.

- Optimized-selenization preparation and laser Q-switching characteristics of layered PtSe2

Qianyong Zhang, Jing Wang, Guoshun Li et al.

J. Phys. B: At. Mol. Opt. Phys. 57 (2024) 225002 (9pp)

https://doi.org/10.1088/1361-6455/ad838a

Measurement-induced heating of a trapped ion

A J Rasmusson¹, Ilyoung Jung¹, Frank G Schroer¹, Antonis Kyprianidis¹ and Philip Richerme^{1,2,*}

- ¹ Indiana University Department of Physics, Bloomington, IN 47405, United States of America
- ² Indiana University Quantum Science and Engineering Center, Bloomington, IN 47405, United States of America

E-mail: richerme@iu.edu

Received 14 July 2024, revised 23 September 2024 Accepted for publication 4 October 2024 Published 15 October 2024



Abstract

We experimentally study the heating of trapped atomic ions during measurement of their internal qubit states. During measurement, ions are projected into one of two basis states and discriminated by their state-dependent fluorescence. We observe that ions in the fluoresceing state rapidly scatter photons and heat at a rate of $\dot{n} \gtrsim 2 \times 10^4$ quanta s⁻¹, which is orders of magnitude faster than typical anomalous ion heating rates. We introduce a quantum trajectory-based framework that accurately reproduces the experimental results and provides a unified description of ion heating for both continuous and discrete sources.

Keywords: measurement-induced, heating, trapped, ion

1. Introduction

A trapped ion heats when it gains motional energy from its surrounding environment. Ion motion is the medium by which quantum information is transferred between qubits [1], and motional heating is detrimental to high-fidelity quantum operations. For instance, heating is known to disrupt the ions' phase space trajectories during the application of entangling operations and necessarily leads to quantum gate errors [2–4]. Moreover, as ions heat, they become even more susceptible to errors arising from non-closure of phase space trajectories, noise in the driving fields, or motional frequency drifts [4–6]. Effects such as anomalous ion heating are so pernicious that they set constraints on ion trap designs [7–9] and entangling gate timings [10, 11], and they motivate specialized preparation of trap electrode surfaces [12, 13] and operation of traps in cryogenic environments [14–16].

Original Content from this work may be used under the terms of the Creative Commons Attribution 4.0 licence. Any further distribution of this work must maintain attribution to the author(s) and the title of the work, journal citation and DOI.

1

Less explored are the heating effects from measurements in the middle of a quantum circuit, which are fundamental to multiple areas of quantum information processing. For instance, many quantum error-correcting protocols rely upon 'mid-circuit' measurements and feedforward to correct errors and provide fault-tolerant operations [17–22]. In addition, mid-circuit measurements are central to measurement-based quantum computing schemes [23, 24] and entanglement phase transitions in quantum many-body systems [25–29]. They may also provide a more efficient way of encoding quantum algorithms on NISO-era hardware [30–32].

Previous work in both trapped-ions and neutral atoms has noticed loss in gate fidelity, or atom loss, due to measurement-induced heating. Consequently, time-consuming recooling schemes were folded into experimental sequences to avoid such detrimental effects [32–36]. However, the specific link between heating processes and mid-circuit measurements, which arise from fundamental photon-atom interactions, have yet to be fully characterized or quantified in trapped-ion systems. Consequently, how much recooling is required to guarantee a given level of error following a mid-circuit measurement was not predictable. Such an understanding would provide a verified model by which to evaluate recooling strategies and estimate potential errors after mid-circuit measurements due to heating.

^{*} Author to whom any correspondence should be addressed.

Here, we experimentally study the measurement-induced heating of a trapped ion. We first establish the anomalous heating rate under ambient conditions, which is then compared to the observed heating rate during measurement of the qubit state. We find a measurement-induced heating rate of $\gtrsim 2 \times 10^4$ quanta s⁻¹, which is ~ 30 times larger than the ambient heating in our trap. We develop a generalized theoretical framework to describe heating from continuous noise sources (leading to anomalous heating) and discrete noise sources (such as photon absorption and emission, responsible for heating during measurement). This framework supports our experimental observation that measurement-induced heating cannot be avoided by specific choices of detection laser parameters. We conclude that dedicated recooling strategies will be required for high-fidelity quantum operations following mid-circuit ion measurements.

2. Ambient heating

Before characterizing the effects of measurement-induced heating, we first measure our baseline ambient heating conditions and introduce a predictive theoretical framework to describe heating in general. Motional state heating \dot{n} is defined as the rate at which the average phonon occupation $\bar{n} = \langle \hat{a}^{\dagger} \hat{a} \rangle$ increases per unit time [8]. Under ambient experimental conditions, \bar{n} will increase due to the interaction of ions with various sources of external noise [8, 37, 38], which generically may be modeled as a continuous, time-dependent fluctuating field [39].

Experiments are performed with a single 171Yb+ ion confined in a four-rod linear Paul trap detailed in [40] with radial secular frequency $\omega = 2\pi \times 1.09$ MHz. Doppler cooling of the ions is accomplished by irradiating the 369.5 nm 2 S_{1/2} $|F=0\rangle \rightarrow ^2$ P_{1/2} $|F=1\rangle$ and 2 S_{1/2} $|F=1\rangle \rightarrow ^2$ P_{1/2} $|F=0\rangle$ transitions, with the dark qubit state $|0\rangle \equiv {}^2S_{1/2}|F=0\rangle$ prepared via optical pumping. Far-detuned Raman beams at 355 nm drive carrier transitions between the hyperfine qubit states $|0\rangle$ and $|1\rangle \equiv {}^2S_{1/2}|F=1$ $m_F=0\rangle$ as well as red and blue sideband transitions [37]. The ion is cooled to near the motional ground state through pulsed resolved sideband cooling using second and first-order red sideband pulses [41]. The internal qubit states are detected by resonantly irradiating the ${}^2S_{1/2}|F=1\rangle \rightarrow {}^2P_{1/2}|F=0\rangle$ transition of the ion at 369.5 nm and collecting the state-dependent fluorescence on a photomultiplier tube for 1 ms. The combined state preparation and measurement errors are estimated to be < 0.3%.

Our measurement of the ambient motional heating rate does not assume that the motional states follow a thermal distribution [41–43] and is executed as follows. The ion is first cooled to near the motional ground state. Then, the ion is left in the dark for a precise delay time gaining motional quanta due to ambient heating sources. A blue sideband is then driven from 0–300 μ s (covering five periods) with 60 time points and 500 repetitions per point. The median value for the low-energy motional state probabilities is then computed using the Singular Value Decomposition (SVD) method [41, 44, 45]

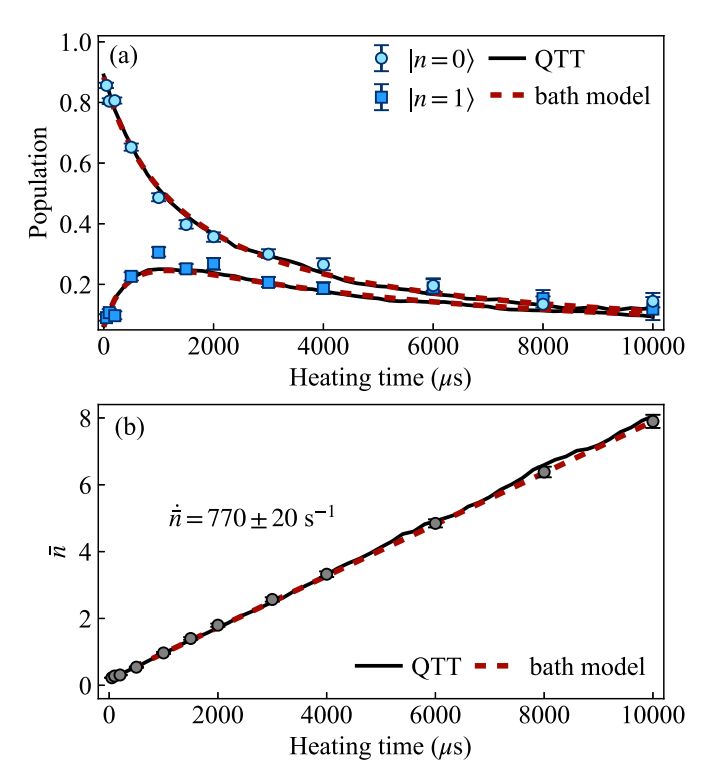


Figure 1. Motional state dynamics under ambient heating conditions. (a) Motional state probabilities are measured using the SVD method. Both a bath model [45] (dashed red) and our Quantum Trajectory Theory (QTT) model (solid black) show good agreement with the experimental data. (b) The estimated \bar{n} under ambient conditions shows linear heating and is well described by both models.

with Monte Carlo error propagation to estimate asymmetric 1σ confidence intervals.

As the delay time for ambient heating is varied, the motional state dynamics under ambient heating conditions are shown in figure 1(a). We plot the occupation probability for the lowest two motional energy levels $|n=0\rangle$ and $|n=1\rangle$ which have the largest dynamic range. Heating dynamics are observed as probability decays out of $|n=0\rangle$ and into $|n=1\rangle$, leading to a temporary increase of the $|n=1\rangle$ probability at early times. Afterwards, population in the states $|n=0\rangle$ and $|n=1\rangle$ monotonically decays towards thermal equilibrium with the environment.

The motional state dynamics may be modeled as an ion coupled to a reservoir, or 'bath', outlined and experimentally observed in [45]. The dynamics of the *n*th diagonal element of the motional state density matrix $\rho_{n,n}(t)$ follow the solution to the master equation for a harmonic oscillator weakly coupled to a high temperature reservoir—which is the case for ambient experimental conditions—and given by [45]

$$\rho_{n,n}(t) = \frac{1}{1+\dot{n}t} \sum_{j=0}^{n} \left(\frac{\dot{\bar{n}}t}{1+\dot{\bar{n}}t}\right)^{j} \left(\frac{1}{1+\dot{\bar{n}}t}\right)^{2n-2j} \times \sum_{l=0}^{\infty} \left(\frac{\dot{\bar{n}}t}{1+\dot{\bar{n}}t}\right)^{l} \times \binom{n+l-j}{n-j} \binom{n}{j} \rho_{n+l-j,n+l-j}(0)$$

$$(1)$$

where \dot{n} is the linear heating rate and the only free parameter. Equation (1) is fit to the measured motional state probabilities, yielding an ambient heating rate of $\dot{n} = 770 \pm 20 \text{ s}^{-1}$. In figure 1(b) we show the estimated \bar{n} from a cumulative fit to the bath model (appendix A). For this data, the initial state after sideband cooling is described by a double thermal distribution, estimated from the initial measured $|n=0\rangle$ and $|n=1\rangle$ values and extended to include the first 100 motional states [41, 42]. Both the data and the bath model exhibit linear heating, as expected for trapped ion systems subject to continuous fluctuations of electric fields.

3. QTT model

We introduce a framework based on semi-classical quantum trajectory theory (QTT) [46, 47] which can accurately predict motional state dynamics, \bar{n} , and $\dot{\bar{n}}$ for both continuous and discrete sources of ion heating. We first describe the approach, then establish its validity for continuous noise sources under ambient heating conditions by comparing it to our experimental data and to the bath model.

Ambient heating sources are modeled as an effective fluctuating electric field E(t) which captures a wide range of physical noise sources [39]. To compute the quantum trajectory along the radial direction of interest, the classical center-of-mass phase space coordinate

$$\alpha(t) = \sqrt{\frac{m\omega}{2\hbar}}\hat{x}(t) + \frac{i}{\sqrt{2m\omega\hbar}}\hat{p}(t)$$
 (2)

with harmonic frequency ω and particle mass m is recorded as E(t) shifts the ion in phase space $\alpha \to \alpha + \alpha_k$. We consider a time interval $\Delta t = t_{k+1} - t_k$ that is long compared to the correlation time of the electric field fluctuations and satisfies $|\alpha_k| \ll 1$. For a fluctuating electric field, a particle of charge e is shifted by [48]

$$\alpha_k = \frac{ie}{\sqrt{2m\omega\hbar}} \int_{t_k}^{t_{k+1}} E(t) e^{i\omega t} dt.$$
 (3)

We then compute the motional state dynamics from the displacement $\hat{D}(\alpha)$ of the initial motional state $|n\rangle$ to Fock state $|m\rangle$. For $m\geqslant n$,

$$p_{m}(n) = |\langle m|\hat{D}(\alpha)|n\rangle|^{2}$$

$$= \frac{n!}{m!} |\alpha|^{2(m-n)} e^{-|\alpha|^{2}} \left[\mathcal{L}_{n}^{(m-n)}(|\alpha|^{2})\right]^{2}$$
(4)

where $\mathcal{L}_n^{(k)}(x)$ is the generalized Laguerre polynomial [49]. Combining this with the definition of α_k in equation (3) (see appendix B), we recover the commonly defined heating rate in the literature [8, 37], $\dot{\bar{n}} = e^2 S_E(\omega)/(4m\omega\hbar)$, where $S_E(\omega)$ is the spectral density of electric field fluctuations at the trap frequency. Quantum trajectories randomly sample electric fields, using a $S_E(\omega)$ independently determined by the bath model, and are averaged together to provide the expected motional heating. On average, the microscopic phase space kicks α_k

are connected to the macroscopic observable \bar{n} since $\langle |\alpha_k|^2 \rangle = \bar{n} \wedge t$

Figure 1 shows that the QTT model, averaged over 1000 trajectories, closely agrees with the experimental data and the bath model in predicting motional state dynamics and \bar{n} . We emphasize that our QTT model contains no adjustable parameters and depends only on the physical quantities in equation (3). In the next section, we will show how QTT may be readily adapted to discrete heating sources, such as photon kicks, by adjusting the definition of α_k accordingly.

4. Measurement-induced heating

We now consider the heating of a trapped ion irradiated with a resonant detection beam, which is the standard configuration for qubit state readout. Two experiments are performed: one where an ion is prepared in the dark qubit state ($|0\rangle$), and a second where an ion is prepared in the bright qubit state ($|1\rangle$). In each case, the ion is first cooled to near its motional ground state by pulsed sideband cooling [41]. If a bright qubit state is desired, we drive a carrier π -pulse from $|0\rangle$ to $|1\rangle$ with measured fidelity 99.3 \pm 0.1 %. The detection beam is then turned on for a variable heating time. An optical pumping pulse then resets the qubit state to $|0\rangle$ while preserving the newly excited phonon state $|n\rangle$. Finally, the phonon state probabilities are measured using the same SVD method outlined in the previous section.

We expect that ions in the dark state will scatter no photons during measurement and exhibit the same heating rate as the ambient case. This expectation is confirmed in figure 2(a), which shows the probability of $|n=0\rangle$ for dark ions during measurement. Data were taken out to 8 ms and fit to a global bath model, yielding an estimated motional heating rate of $780 \pm 40 \text{ s}^{-1}$. This rate is indistinguishable from the ambient case presented in figure 1(b) $(770 \pm 20 \text{ s}^{-1})$.

In stark contrast, ions in the bright qubit state will undergo stochastic momentum kicks of order $\sim \hbar k$ due to photon absorption and emission. This process cannot be generically described by the bath model of equation (1). Although photon scattering does not increase the average velocity of the ion ($\langle v \rangle = 0$ in a trap), the stochastic timing of photon recoil events relative to the harmonic motion of the ion is expected to increase velocity fluctuations $\langle v^2 \rangle$ and therefore increase motional energy [50]. This mechanism is observed in figure 2(b) where the $|n=0\rangle$ probability of a prepared bright ion decays rapidly, indicating fast heating out of the motional ground state.

We model this process using our QTT framework, where the phase-space kick α_k now encodes the effects of atomic scattering processes. We write (appendix C):

$$\alpha_k = \frac{i e^{i\omega t} \hbar k}{\sqrt{2m\omega\hbar}} \left[\sqrt{f_x} + \sqrt{f_{sx}^{(k)}} + \frac{8\sqrt{f_x}\Delta\omega n}{\gamma^2 (1+s') + 4\Delta^2} \right]$$
 (5)

where $\omega = 2\pi \times 1.09$ MHz is the trap frequency along the radial x-axis, $k = 2\pi/(369.5 \text{ nm})$ is the wave vector, and n is the ion motional state. In equation (5), absorption is described

by the geometric factor $f_x = 1/4$ which accounts for the projection of the incident laser beam along the x-axis. Emission is treated with geometric factor $f_{xx}^{(k)}$, randomly chosen to recreate an isotropic emission pattern [47, 50]. Finally, the Doppler effect is included as the final term in equation (5) and depends on parameters such as the natural linewidth γ , modified saturation parameter s', and laser detuning Δ [51].

The overall measurement-induced heating rate is given by the average energy gained per scattering event, $\hbar\omega|\alpha_k|^2$, times the scattering rate Γ . We determine Γ by fitting a measured fluorescence versus intensity curve to the scattering rate equation appropriate for $^{171}\mathrm{Yb}^+$ [51]

$$\Gamma = \frac{\gamma (s/18)}{1 + \frac{1}{216} \left(\frac{s\gamma}{\delta_B}\right)^2 + \frac{8}{3} \left(\frac{\delta_B}{\gamma}\right)^2 + \left(\frac{2\Delta}{\gamma}\right)^2} \tag{6}$$

where $s \equiv I/I_{\rm sat}$ is the saturation parameter for the detection transition at 369 nm, Δ is the laser detuning, $\gamma = 2\pi \times 19.6$ MHz is the natural linewidth, and $\delta_B = 2\pi \times 5.288$ MHz is the Zeeman splitting. For the saturation parameter $s = 1.27 \pm 0.02$ used in these experiments, the corresponding scattering rate is $\Gamma = 2\pi \times (1.07 \pm 0.01)$ MHz, with the error arising predominantly from uncertainty in s. Consequently, the QTT model inherits this uncertainty in s and Γ when predicting the motional heating rate $\dot{\bar{n}}$.

We report agreement between the QTT model and the experimental data to within error bars in figure 2. The model accurately predicts the dynamics of the motional ground state (figures 2(a) and (b)) and all measured low-lying motional states (figure 2(c)). This agreement at short times is particularly noteworthy, since most heating models assume thermal state distributions and would fail to capture the initial non-thermal behavior following sideband cooling [41–43]. As before, the QTT model in figure 2 contains no adjustable parameters and depends only on the independently-measured scattering rate, atomic physics, and the laser properties described in equation (5).

Figure 2(d) shows the rapid increase in \bar{n} during measurement-induced heating. The QTT prediction (dark blue line) shows a linear heating rate of $\dot{\bar{n}} = 22900 \pm 240$ s⁻¹, which is nearly 30 times faster than the heating rate for ions in the dark state or under ambient heating conditions. For comparison, we also fit the measured low-energy states $|n=0\rangle$, $|n=1\rangle$, and $|n=2\rangle$ to a presumed thermal distribution at each time point (dashed black line). The thermal fit significantly underestimates \bar{n} at early times, consistent with previous numeric simulations and experimental observations [41–43] and only matches the experimental data after several hundred scattering events have taken place.

Since the typical qubit measurement time for trapped ions is significantly longer than the 100 μ s timescale shown in figures 2(c) and (d), we investigate whether this rapid linear heating persists at longer times. As seen in equation (5), the choice of laser detuning Δ plays a key role in determining the

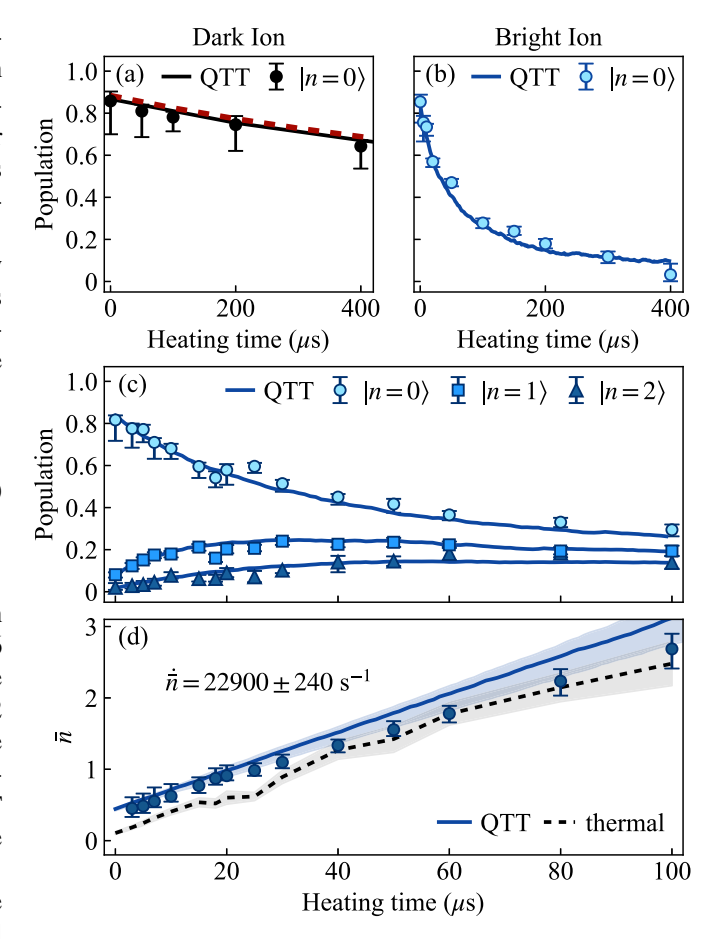


Figure 2. Motional state dynamics during measurement-induced heating. (a) Motional ground state $|n=0\rangle$ probability for a dark ion. The bath model (dashed red) under the ambient conditions of figure 1(a) is included for comparison. (b) The motional ground state probability for bright-state ions decays much more rapidly than for dark-state ions. (c) Early-time population dynamics of a bright ion undergoing measurement-induced heating. The QTT model accurately describes the data with no adjustable parameters. (d) Estimates of \bar{n} based on the panel (c) data, comparing the QTT model to a thermal model. Shaded bands indicate 1σ model uncertainties. Errors in the QTT model arise from experimental measurement errors in the scattering rate Γ .

typical magnitude of phase-space kicks during photon scattering. Therefore, we study measurement-induced heating in the long-time limit for three different choices of Δ , spanning the red-detuned, near-resonant, and blue-detuned regimes.

When the average ion energy exceeds $\bar{n} \approx 10$, it becomes difficult for traditional sideband thermometry techniques to accurately measure the motional state [37, 41, 52]. For this reason, we use a carrier Rabi oscillation to estimate \bar{n} after extended heating times of up to 2 ms. Following measurement-induced heating of the trapped ion, a carrier oscillation is driven from 0 to 40 μ s (covering 6 periods) with 60 time points and 300 repetitions each. The carrier oscillation is fit with \bar{n} as a free parameter, taking into account all appropriate Debye-Waller factors (see appendix E) [37]. This fitting procedure assumes a thermal motional state distribution, which is in agreement with our data after \sim 50 μ s (figure 2(d)).

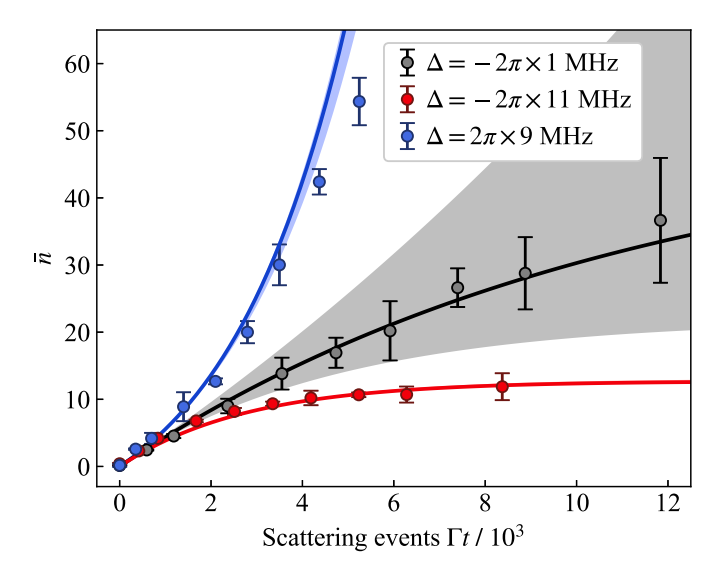


Figure 3. Measurement-induced heating depends sensitively on the detuning Δ of the detection beam. Darker solid lines are predicted values according to equation (7) with shaded areas showing \pm 2 MHz uncertainty bands in detuning. Points and lines of the same color have the same detuning.

Figure 3 shows the sensitivity of ion motional heating to laser detuning Δ in the long-time limit. We perform the experiment with three different detection beam detunings: $\Delta = 2\pi \times \{-11, -1, 9\}$ MHz, corresponding to red-detuned, near-resonant, and blue-detuned, respectively. In figure 3, the x-axis is scaled by the photon scattering rate of each detuning, $\Gamma = 2\pi \times \{0.56, 0.94, 0.67\}$ MHz as calculated from the scattering rate for 171 Yb+ provided in equation (6) [51]. Our typical state detection requires $\Gamma t \approx 5 \times 10^3$ scattering events. For the red-detuned case, where Δ is chosen near the optimal Doppler detuning, the data equilibrates to the Doppler cooling limit $\bar{n} \approx 12.7$. All other choices for Δ leave the ion with higher motional energy in the long-time limit.

The expected $\bar{n}(t)$ under these conditions may be predicted by extending the QTT model with equation (5) to long times, or by adapting the equations governing laser cooling [50] to describe measurement-induced heating. We find (appendix D):

$$\bar{n}(t) = \left[\left(\bar{n}(0) - \frac{R}{D\hbar\omega} \right) e^{-\Gamma_0 Dt} + \frac{R}{D\hbar\omega} \right]$$
 (7)

where we define $\Gamma_0 \equiv \gamma(s/18)/(1+s'+4\Delta^2/\gamma^2)$ as the effective scattering rate, $R \equiv (f_x+f_{sx})\hbar^2k^2/(2m)$ as the effective recoil energy, and $D \equiv 8\Delta\hbar f_x k^2/(m\gamma^2(1+s')+4m\Delta^2)$ as a Doppler-effect term that takes into account the laser detuning Δ . In the expressions above, we assume that spontaneous emission is isotropic $(f_{sx}=1/3)$ and that the initial Doppler shift $\vec{k}\cdot\vec{v}$ is small compared to the natural linewidth γ . The parameters in equation (7) are independently measured, and the predicted curves for each detuning are plotted as solid lines in figure 3. Shaded bands illustrate our ± 2 MHz experimental uncertainty in measuring Δ .

From this model and the data in figure 3, we find that rapid measurement-induced heating cannot be avoided by judicious choice of detection beam parameters. At the start of a measurement, the short-time behavior of equation (7) may be approximated as $\bar{n}(t) \approx \bar{n}(0) + \Gamma_0 R t/(\hbar \omega)$. This corresponds to linear initial heating at rate $\dot{\bar{n}} = \Gamma_0 R/(\hbar \omega) \sim 2 \times 10^4 \text{ s}^{-1}$, in agreement with measurements in figure 2(d). The only tunable beam parameter is the photon scattering rate Γ_0 , which cannot be reduced without sacrificing the qubit state detection fidelity or increasing the detection time (leading to the same final \bar{n}). We also note that this measurement-induced heating rate in $^{171}\text{Yb}^+$ is among the *smallest* for common trapped-ion species, since the effective recoil energy R, and hence \bar{n} , are suppressed by the large ion mass.

Discussion and outlook—Mid-circuit measurements will be a critical element to future quantum technologies. This work has quantified the rapid motional heating which takes place during the measurement of a trapped ion, which dominates over anomalous heating and is an unavoidable consequence of photon scattering. We have also provided a unified framework (QTT) to accurately model motional heating effects for both continuous and discrete noise sources. Our experimental data and theoretical modeling indicate that, if left unmitigated, measurement-induced heating will present a substantial roadblock for performing high-fidelity operations following a mid-circuit measurement.

The effects of measurement-induced heating become more complex when detecting the state of specific ions in a larger array. For a collection of co-trapped ions, measurement-induced heating will add motional energy to all vibrational modes in which a bright ion participates, weighted by their mode participation amplitudes. Thus, measurement of a single ion within an array may demand recooling of multiple vibrational modes before high-fidelity gate operations may proceed.

We conclude that for mid-circuit measurements to be viable, dedicated mid-circuit recooling strategies must be implemented to combat measurement-induced heating. Brute-force sympathetic cooling has been successful at reducing multiple sources of ion heating, at the cost of co-trapping multiple ion species and spending more time recooling than executing quantum gate operations [32, 34]. More sophisticated recooling schemes may be needed, such as rapid exchange cooling [53], phonon rapid adiabatic passage cooling [54], or perhaps dedicated mid-circuit measurement zones within a QCCD trap [34, 55]. Future work may also consider simultaneous ion measurement and recooling by utilizing shelving, state teleportation [56], or the *omg* qubit architecture [57].

Data availability statement

The data cannot be made publicly available upon publication because no suitable repository exists for hosting data in this field of study. The data that support the findings of this study are available upon reasonable request from the authors.

Acknowledgments

This material was based on work supported by the U.S. National Science Foundation, under Grant CHE-2311165. The IUB Quantum Science and Engineering Center is supported by the Office of the Vice Provost for Research through its EAR program.

Appendix A. Determination of \bar{n} from the bath model

To estimate \bar{n} , we describe the initial motional state by a double thermal distribution, estimated from the initial measured $|n=0\rangle$ and $|n=1\rangle$ values and extended to include the first 100 motional states [41, 42]. We then compute multiple fits of the motional heating rate \bar{n} to the data using the bath model. A cumulative fit is used for each point, such that \bar{n}_k determined at the kth time point only includes data up to time t_k . Each heating rate \bar{n}_k is then used to propagate the initial motional state following the bath model dynamics, resulting in an estimate of \bar{n} at time t_k .

Appendix B. Derivation of continuous heating rate from QTT model

To compute the semi-classical quantum trajectories, the classical center-of-mass phase space coordinate

$$\alpha(t) = \sqrt{\frac{m\omega}{2\hbar}}\hat{x}(t) + \frac{i}{\sqrt{2m\omega\hbar}}\hat{p}(t)$$
 (8)

is recorded as external sources stochastically shift $\alpha \to \alpha + \alpha_k$ over a small time interval $\Delta t = t_{k+1} - t_k$, such that $\alpha_k \ll 1$ [46, 47]. Ambient heating sources are modeled as an effective fluctuating electric field E(t), which captures a wide range of physical noise sources [39]. For a fluctuating electric field, a particle of charge e is shifted by [48]

$$\alpha_k = \frac{ie}{\sqrt{2m\omega\hbar}} \int_{t_k}^{t_{k+1}} E(t') e^{i\omega t'} dt'. \tag{9}$$

As stated in the main text, we then compute the motional state dynamics from the displacement $\hat{D}(\alpha)$ of the initial motional state $|n\rangle$ to Fock state $|m\rangle$ with $m \ge n$:

$$p_{m}(n) = |\langle m|\hat{D}(\alpha)|n\rangle|^{2}$$

$$= \frac{n!}{m!} |\alpha|^{2(m-n)} e^{-|\alpha|^{2}} \left[\mathcal{L}_{n}^{(m-n)}(|\alpha|^{2})\right]^{2}. \quad (10)$$

We observe that this probability depends on the square of the phase space displacement, $|\alpha|^2$. From our definition of α_k , the square of the phase space kick is:

$$|\alpha_k|^2 = \frac{e^2}{2m\hbar\omega} \left| \int_{t_k}^{t_{k+1}} E(t') e^{i\omega t'} dt' \right|^2. \tag{11}$$

Following Savard [58], and using the Wiener-Khinchin theorem for time averages where the autocorrelation function decays to zero for long times, the squared integral on the right-hand side may be replaced by an integral over the autocorrelation of the electric field fluctuations:

$$|\alpha_k|^2 = \frac{e^2}{2m\hbar\omega} \Delta t \int_{-\infty}^{\infty} d\tau e^{i\omega\tau} \langle E(t)E(t+\tau) \rangle . \tag{12}$$

Finally, under the definition of the single-sided spectral density of electric field fluctuations [59],

$$S_{E}(\omega) = 2 \int_{-\infty}^{\infty} d\tau e^{i\omega\tau} \langle E(t)E(t+\tau) \rangle$$
 (13)

we can rewrite equation (12) in terms of the spectral density of electric field noise:

$$|\alpha_k|^2 = \frac{e^2}{4m\hbar\omega} S_E(\omega) \Delta t = \dot{\bar{n}} \Delta t.$$
 (14)

Appendix C. Derivation of discrete heating rate from QTT model

Here, we calculate the change in phase space coordinate due to discrete photon scattering events. Near-resonance incident photons apply an average force on 171 Yb⁺ in the x-direction, quoted from [50] as

$$\langle F_x \rangle = \Gamma_0 \hbar k \sqrt{f_x} \left(1 + \frac{8\Delta n\omega}{\gamma^2 (1 + s') + 4\Delta^2} \right)$$
 (15)

with variable definitions matching those given the text. The scattering rate appropriate for ¹⁷¹Yb⁺ is [51]

$$\Gamma_0 = \frac{\gamma (s/18)}{1 + s' + \frac{4\Delta^2}{\gamma^2}} \,. \tag{16}$$

where the natural line width $\gamma = 2\pi \times 19.6$ MHz, and

$$s' = \frac{1}{216} \left(\frac{s\gamma}{\delta_B} \right)^2 + \frac{8}{3} \left(\frac{\delta_B}{\gamma} \right)^2 \tag{17}$$

where in our experiments the Zeeman splitting is $\delta_B = 2\pi \times 5.288$ MHz and the saturation parameter s = 1.27.

The momentum kick per absorption event $\Delta p_{\rm abs}$ includes the Doppler related frequency shifts

$$\Delta p_{\text{abs}} = \hbar k \sqrt{f_x} \left(1 + \frac{8\Delta n\omega}{\gamma^2 (1 + s') + 4\Delta^2} \right) . \tag{18}$$

Momentum kicks due to emission are independent of velocity, delivering a momentum change

$$\Delta p_{\rm em} = \hbar k \sin(\theta) \cos(\phi) \tag{19}$$

with angles θ and ϕ randomly chosen to generate an isotropic emission pattern [50].

The change in phase space α_k due to a photon scattering event (absorption and emission) then is calculated as

$$\alpha_{k} = \frac{ie^{i\omega t}}{\sqrt{2m\omega\hbar}} \Delta p$$

$$\alpha_{k} = \frac{ie^{i\omega t}\hbar k}{\sqrt{2m\omega\hbar}} \left[\sqrt{f_{x}} \left(1 + \frac{8\Delta n\omega}{\gamma^{2} (1+s') + 4\Delta^{2}} \right) + \sin(\theta)\cos(\phi) \right]$$
(20)

where the change in α due to absorption events has already been averaged over while the change in α due to emission will be averaged over in the quantum trajectory Monte Carlo. A single scattering event is on the order of 10 ns while the trap period is 1 μ s. Therefore, we have assumed the same phase for an absorption-emission event pair.

This microscopic calculation of α_k generates the exact same heating dynamics \dot{n} as the more common semi-classical Doppler shifted energy equations [50] as will be shown below. The average motional energy $E = \hbar \omega |\alpha_k|^2$ is given by

$$E = \frac{\hbar^2 k^2}{2m} \left[f_x \left(1 + \frac{8\Delta n\omega}{\gamma^2 (1 + s') + 4\Delta^2} \right)^2 + f_{sx} \right]$$
(21)

where the isotropic emission geometry factor $f_{sx} = \langle \sin(\theta)^2 \cos(\phi^2) \rangle = 1/3$. Applying the binomial approximation, the average motional energy E of equation (21) recovers the result from the semi-classical Doppler derivation.

$$E = \left[\frac{\hbar^2 k^2}{2m} \left(f_x + f_{sx} \right) + \frac{8\Delta \hbar f_x k^2 / m}{\gamma^2 \left(1 + s' \right) + 4\Delta^2} n\hbar \omega \right] . \tag{22}$$

This approach is in complete agreement with the semi-classical analysis. The energy change per scattering event is given by $\hbar\omega|\alpha_k|^2$, and the total rate of energy change $\mathrm{d}E/\mathrm{d}t=\Gamma_0\hbar\omega|\alpha_k|^2$. Comparing this expression with the semi-classical calculation for $\mathrm{d}E/\mathrm{d}t$ (equation (28) below), we arrive at the same result having started from a microscopic phase space displacement picture.

Appendix D. Semi-classical laser heating

We consider the regime where a near-resonant laser irradiating a harmonically trapped atom can cause heating of the ion's motion. Our treatment initially follows [50] but then deviates to consider the case of heating due to the laser frequency being near-resonance or blue-detuned ($\Delta > 0$).

Consider a resonant beam of intensity I and wavevector \vec{k} . When this light hits a trapped ion moving with velocity \vec{v} and a photon is absorbed, a photon is later emitted with wavevector \vec{k}_s .

To find the energy rate of change along a direction of interest (i.e. x-axis), we multiply the change in energy by the

scattering rate $\Gamma(\omega, \vec{v})$ and average over the absorption and emission scattering directions:

$$\frac{\mathrm{d}E_x}{\mathrm{d}t} = \left\langle \Gamma\left(\omega, \vec{v}\right) \left[\frac{\hbar^2 k^2}{2m} \left(f_x + f_{sx} \right) + \hbar k_x v_x \right] \right\rangle \tag{23}$$

where m is the mass of the trapped ion, v_x is the velocity in along the x-axis, k is the magnitude of \vec{k} , $f_x = \hat{k}_x^2$ is the incident photon geometric factor along the x-direction, and $f_{sx} = \hat{k}_{sx}^2$ is the emitted photon geometric factor along the x-direction.

The scattering rate $\Gamma(\omega, \vec{v})$ from [51, 60] is given by:

$$\Gamma(\omega, \vec{v}) = \frac{\gamma(s/18)}{1 + s' + \frac{4(\Delta + \vec{k} \cdot \vec{v})^2}{\gamma^2}}$$
(24)

where $\gamma = 2\pi \times 19.6$ MHz is the natural linewidth, $s = I/I_{sat}$ is the saturation parameter, Δ is the detuning from resonance, and

$$s' = \frac{1}{216} \left(\frac{s\gamma}{\delta_B} \right)^2 + \frac{8}{3} \left(\frac{\delta_B}{\gamma} \right)^2 \tag{25}$$

with Zeeman splitting δ_B .

The Doppler shift $\vec{k} \cdot \vec{v}$ is much smaller than the natural linewidth such that equation (24) may be approximated by

$$\Gamma(\omega, \vec{v}) \approx \Gamma_0 \left[1 + \frac{8\Delta \left(\vec{k} \cdot \vec{v} \right)}{\gamma^2 \left(1 + s' \right) + 4\Delta^2} \right]$$
 (26)

where

$$\Gamma_0 = \frac{\gamma (s/18)}{1 + s' + \frac{4\Delta^2}{\gamma^2}} \,. \tag{27}$$

The change in energy (equation (23)), assuming $\langle v_i \rangle = 0$ and $\langle v_i v_j \rangle = 0$ for any two directions $i \neq j$, becomes

$$\frac{\mathrm{d}E_x}{\mathrm{d}t} = \Gamma_0 \left[\frac{\hbar^2 k^2}{2m} \left(f_x + f_{sx} \right) + \frac{8\Delta \hbar f_x k^2 E_x / m}{\gamma^2 \left(1 + s' \right) + 4\Delta^2} \right] \tag{28}$$

where the average classical harmonic oscillator energy $E_x = m\langle v_x^2 \rangle$ has been swapped in (with no factor of 1/2).

Equation (28) is a first order differential equation which can be solved analytically. For convenience, we define:

$$R \equiv \frac{\hbar^2 k^2}{2m} \left(f_x + f_{sx} \right) \tag{29}$$

$$D \equiv \frac{8\Delta\hbar f_x k^2/m}{\gamma^2 (1+s') + 4\Delta^2}$$
 (30)

then our equation may be written

$$\frac{\mathrm{d}E_x}{\mathrm{d}t} = \Gamma_0 \left(R - DE_x \right) \tag{31}$$

which has the solution

$$E_x(t) = \left(E_x(0) - \frac{R}{D}\right)e^{-\Gamma_0 Dt} + \frac{R}{D}.$$
 (32)

Replacing the energy with the average motional state $\bar{n} = E_x(t)/(\hbar\omega)$, we arrive at equation in the main text.

We examine equation (32) in a few limits. First, in the long-time limit, the final value of the energy converges to:

$$E_x(\infty) = \frac{R}{D} = \frac{\hbar \gamma}{8} \left(1 + \frac{f_{sx}}{f_x} \right) \left[\frac{\gamma (1 + s')}{2\Delta} + \frac{2\Delta}{\gamma} \right]. \quad (33)$$

This agrees with results in the literature [61], which are typically derived by setting $dE_x/dt = 0$ in equation (28).

Another limit is the special case of zero detuning (D=0). In the limit of $D \to 0$, the motional energy is readily given by:

$$E_x(t) = E_x(0) + \Gamma_0 Rt$$
. (34)

With no damping force from cooling ($\Delta = 0$), the ion experiences linear heating at constant rate $\Gamma_0 R$.

Appendix E. High \bar{n} measurement

We estimate \bar{n} for heating times up to 2 ms using a measured carrier Rabi oscillation. In these experiments, the ion is first prepared near its motional ground state. A carrier π -pulse then prepares a bright qubit state; the ion is then irradiated by the detection beam for a variable length of time, extending out to 2 ms.

Far-detuned 355 nm Raman beams couple to the x and y principal axes in this experiment, so both modes affect the carrier Rabi oscillation. A carrier Rabi oscillation with x and y COM mode couplings is given by

$$P_{\text{bright}}(t) = \sum_{n_x, n_y=0}^{\infty} p_{n_x} p_{n_y} \sin\left(\Omega_{n_x, n_y} t/2\right)^2$$
 (35)

where the Rabi frequency for the x and y mode couplings is given by

$$\Omega_{n_x,n_y} = \Omega_0 e^{-\eta_x^2/2} e^{-\eta_y^2/2} \mathcal{L}_{n_x} (\eta_x^2) \mathcal{L}_{n_y} (\eta_y^2)$$
 (36)

with $\eta_x = 0.104$ and $\eta_y = 0.112$ measured independently [37]. The thermal contribution from the y-axis can be removed by approximating its contribution with the ratio of the respective secular frequencies $\bar{n}_y = (\omega_x/\omega_y)\bar{n}_x = 1.48\bar{n}_x$. The motional distribution is assumed to be thermal. The final fitting parameters of the measured carrier Rabi oscillation are then the Rabi frequency and average motional state along the x-axis, $\{\Omega_0, \bar{n}_x\}$.

ORCID iDs

A J Rasmusson https://orcid.org/0000-0002-7774-242X Ilyoung Jung https://orcid.org/0009-0005-3956-4932 Frank G Schroer https://orcid.org/0009-0005-7922-5345 Philip Richerme https://orcid.org/0000-0003-1799-7612

References

- Mølmer K and Sørensen A 1999 Multiparticle entanglement of hot trapped ions *Phys. Rev. Lett.* 82 1835
- [2] Haddadfarshi F and Mintert F 2016 High fidelity quantum gates of trapped ions in the presence of motional heating New J. Phys. 18 123007
- [3] Milne A R, Edmunds C L, Hempel C, Roy F, Mavadia S and Biercuk M J 2020 Phase-modulated entangling gates robust to static and time-varying errors *Phys. Rev. Appl.* 13 024022
- [4] Valahu C H, Apostolatos I, Weidt S and Hensinger W K 2022 Quantum control methods for robust entanglement of trapped ions J. Phys. B: At. Mol. Opt. Phys. 55 204003
- [5] Bentley C D B, Ball H, Biercuk M J, Carvalho A R R, Hush M R and Slatyer H J 2020 Numeric optimization for configurable, parallel, error-robust entangling gates in large ion registers Adv. Quantum Technol. 3 2000044
- [6] Cetina M, Egan L N, Noel C, Goldman M L, Biswas D, Risinger A R, Zhu D and Monroe C 2022 Control of transverse motion for quantum gates on individually addressed atomic qubits PRX Quantum 3 010334
- [7] Deslauriers L, Olmschenk S, Stick D, Hensinger W K, Sterk J and Monroe C 2006 Scaling and suppression of anomalous heating in ion traps *Phys. Rev. Lett.* 97 103007
- [8] Brownnutt M, Kumph M, Rabl P and Blatt R 2015 Ion-trap measurements of electric-field noise near surfaces *Rev. Mod. Phys.* 87 1419
- [9] An D, Matthiesen C, Urban E and H\u00e4ffner H 2019 Distance scaling and polarization of electric-field noise in a surface ion trap *Phys. Rev.* A 100 063405
- [10] Ballance C J, Harty T P, Linke N M, Sepiol M A and Lucas D M 2016 High-fidelity quantum logic gates using trapped-ion hyperfine qubits *Phys. Rev. Lett.* 117 060504
- [11] Gaebler J P *et al* 2016 High-fidelity universal gate set for be 9+ ion qubits *Phys. Rev. Lett.* **117** 060505
- [12] Allcock D T C, Guidoni L, Harty T P, Ballance C J, Blain M G, Steane A M and Lucas D M 2011 Reduction of heating rate in a microfabricated ion trap by pulsed-laser cleaning *New J. Phys.* 13 123023
- [13] Hite D A et al 2012 100-fold reduction of electric-field noise in an ion trap cleaned with in situ argon-ion-beam bombardment Phys. Rev. Lett. 109 103001
- [14] Labaziewicz J Y, Antohi P, Leibrandt D, Brown K R and Chuang I L 2008 Suppression of heating rates in cryogenic surface-electrode ion traps *Phys. Rev. Lett.* 100 013001
- [15] Pagano G et al 2018 Cryogenic trapped-ion system for large scale quantum simulation Quantum Sci. Technol. 4 014004
- [16] Weber M A, Löschnauer C, Wolf J, Gely M F, Hanley R K, Goodwin J F, Ballance C J, Harty T P and Lucas D M 2023 Cryogenic ion trap system for high-fidelity near-field microwave-driven quantum logic *Quantum Sci. Technol*. 9 015007
- [17] Chiaverini J et al 2004 Realization of quantum error correction Nature 432 602–5
- [18] Terhal B M 2015 Quantum error correction for quantum memories Rev. Mod. Phys. 87 307
- [19] Negnevitsky V, Marinelli M, Mehta K K, Lo H-Y, Flühmann C and Home J P 2018 Repeated multi-qubit readout and feedback with a mixed-species trapped-ion register *Nature* 563 527–31
- [20] Wan Y et al 2019 Quantum gate teleportation between separated qubits in a trapped-ion processor Science 364 875–8
- [21] Ryan-Anderson C et al 2021 Realization of real-time fault-tolerant quantum error correction Phys. Rev. X 11 041058
- [22] Postler L, Butt F, Pogorelov I, Marciniak C D, Heußen S, Blatt R, Schindler P, Rispler M, Müller M and Monz T 2024

- Demonstration of fault-tolerant steane quantum error correction *PRX Quantum* **5** 030326
- [23] Raussendorf R, Browne D E and Briegel H J 2003 Measurement-based quantum computation on cluster states *Phys. Rev.* A 68 022312
- [24] Briegel H J, Browne D E, Dür W, Raussendorf R and Van den Nest M 2009 Measurement-based quantum computation Nat. Phys. 5 19–26
- [25] Iqbal M, Tantivasadakarn N, Gatterman T M, Gerber J A, Gilmore K, Gresh D, Hankin A, Hewitt N, Horst C V and Matheny M 2024 Topological order from measurements and feed-forward on a trapped ion quantum computer Commun. Phys. 7 205
- [26] Iqbal M, Tantivasadakarn N, Verresen R, Campbell S L, Dreiling J M, Figgatt C, Gaebler J P, Johansen J, Mills M and Moses S A 2024 Non-abelian topological order and anyons on a trapped-ion processor *Nature* 626 505–11
- [27] Skinner B, Ruhman J and Nahum A 2019 Measurement-induced phase transitions in the dynamics of entanglement *Phys. Rev.* X 9 031009
- [28] Ippoliti M, Gullans M J, Gopalakrishnan S, Huse D A and Khemani V 2021 Entanglement phase transitions in measurement-only dynamics *Phys. Rev.* X 11 011030
- [29] Foss-Feig M, Tikku A, Lu T-C, Mayer K, Iqbal M, Gatterman T M, Gerber J A, Gilmore K, Gresh D and Hankin A 2023 Experimental demonstration of the advantage of adaptive quantum circuits (arXiv:2302.03029)
- [30] Chertkov E et al 2022 Holographic dynamics simulations with a trapped-ion quantum computer Nat. Phys. 18 1074–9
- [31] DeCross M, Chertkov E, Kohagen M and Foss-Feig M 2023 Qubit-reuse compilation with mid-circuit measurement and reset *Phys. Rev.* X 13 041057
- [32] Moses S A et al 2023 A race-track trapped-ion quantum processor Phys. Rev. X 13 041052
- [33] Schindler P, Monz T, Nigg D, Barreiro J T, Martinez E A, Brandl M F, Chwalla M, Hennrich M and Blatt R 2013 Undoing a quantum measurement *Phys. Rev. Lett.* 110 070403
- [34] Pino J M, Dreiling J M, Figgatt C, Gaebler J P, Moses S A, Allman M S, Baldwin C H, Foss-Feig M, Hayes D and Mayer K 2021 Demonstration of the trapped-ion quantum CCD computer architecture *Nature* 592 209–13
- [35] Covey J P, Madjarov I S, Cooper A and Endres M 2019 2000-times repeated imaging of strontium atoms in clock-magic tweezer arrays *Phys. Rev. Lett.* 122 173201
- [36] Chow M N H, Little B J and Jau Y-Y 2023 High-fidelity low-loss state detection of alkali-metal atoms in optical tweezer traps *Phys. Rev.* A 108 032407
- [37] Wineland D J, Monroe C, Itano W M, Leibfried D, King B E and Meekhof D M 1998 Experimental issues in coherent quantum-state manipulation of trapped atomic ions *J. Res. Natl Inst. Stand. Technol.* **103** 259
- [38] Hite D A, McKay K S, Kotler S, Leibfried D, Wineland D J and Pappas D P 2017 Measurements of trapped-ion heating rates with exchangeable surfaces in close proximity MRS Adv. 2 2189–97
- [39] Lamoreaux S K 1997 Thermalization of trapped ions: a quantum perturbation approach Phys. Rev. A 56 4970
- [40] D'Onofrio M, Xie Y, Rasmusson A J, Wolanski E, Cui J and Richerme P 2021 Radial two-dimensional ion crystals in a linear paul trap *Phys. Rev. Lett.* 127 020503

- [41] Rasmusson A J, D'Onofrio M, Xie Y, Cui J and Richerme P 2021 Optimized pulsed sideband cooling and enhanced thermometry of trapped ions *Phys. Rev.* A 104 043108
- [42] Chen J-S, Brewer S M, Chou C W, Wineland D J, Leibrandt D R and Hume D B 2017 Sympathetic ground state cooling and time-dilation shifts in an al 27+ optical clock *Phys. Rev. Lett.* 118 053002
- [43] Reed E C, Qi L and Brown K R 2024 Comparison of continuous and pulsed sideband cooling on an electric quadrupole transition *Phys. Rev.* A 110 013123
- [44] Meekhof D M, Monroe C, King B E, Itano W M and Wineland D J 1996 Generation of nonclassical motional states of a trapped atom *Phys. Rev. Lett.* **76** 1796
- [45] Turchette Q A, Myatt C J, King B E, Sackett C A, Kielpinski D, Itano W M, Monroe C and Wineland D J 2000 Decoherence and decay of motional quantum states of a trapped atom coupled to engineered reservoirs *Phys. Rev.* A 62 053807
- [46] Carmichael H J 2007 Statistical Methods in Quantum Optics 2: Non-Classical Fields (Springer)
- [47] Horvath L, Collett M J, Carmichael H J and Fisher R 2007 Quantum stochastic heating of a trapped ion Conf. on Coherence and Quantum Optics CTuE (Optica Publishing Group) p 2
- [48] James. D F V 1998 Theory of heating of the quantum ground state of trapped ions *Phys. Rev. Lett.* **81** 317
- [49] De Oliveira F A M, Kim M S, Knight P L and Buek V 1990 Properties of displaced number states *Phys. Rev.* A 41 2645
- [50] Itano W M and Wineland D J 1982 Laser cooling of ions stored in harmonic and penning traps Phys. Rev. A 25 35
- [51] Ejtemaee S, Thomas R and Haljan P C 2010 Optimization of Yb+ fluorescence and hyperfine-qubit detection *Phys. Rev.* A 82 063419
- [52] Diedrich F, Bergquist J C, Itano W M and Wineland D J 1989 Laser cooling to the zero-point energy of motion *Phys. Rev. Lett.* 62 403
- [53] Fallek S D, Sandhu V S, McGill R A, Gray J M, Tinkey H N, Clark C R and Brown K R 2024 Rapid exchange cooling with trapped ions *Nat. Commun.* 15 1089
- [54] Fabrikant M I, Lauria P, Madjarov I S, Burton W C and Sutherland R T 2024 Cooling trapped ions with phonon rapid adiabatic passage (arXiv:2403.02315)
- [55] Kielpinski D, Monroe C and Wineland D J 2002 Architecture for a large-scale ion-trap quantum computer *Nature* 417 709–11
- [56] Schmidt P O, Rosenband T, Langer C, Itano W M, Bergquist J C and Wineland D J 2005 Spectroscopy using quantum logic Science 309 749–52
- [57] Allcock D T C, Campbell W C, Chiaverini J, Chuang I L, Hudson E R, Moore I D, Ransford A, Roman C, Sage J M and Wineland D J 2021 OMG blueprint for trapped ion quantum computing with metastable states *Appl. Phys. Lett.* 119 214002
- [58] Savard T A, O'hara K M and Thomas J E 1997 Laser-noise-induced heating in far-off resonance optical traps *Phys. Rev.* A 56 R1095
- [59] Turchette Q A *et al* 2000 Heating of trapped ions from the quantum ground state *Phys. Rev.* A **61** 063418
- [60] Berkeland D J and Boshier M G 2002 Destabilization of dark states and optical spectroscopy in zeeman-degenerate atomic systems *Phys. Rev.* A 65 033413
- [61] Leibfried D, Blatt R, Monroe C and Wineland D 2003 Quantum dynamics of single trapped ions *Rev. Mod. Phys.* 75 281